RISK OF COLLISION FOR THE NAVIGATION CONSTELLATIONS: THE CASE OF THE FORTHCOMING GALILEO

A. Rossi*, G.B. Valsecchi† and E. Perozzi‡

Sommario

The satellite global positioning systems presently in space are the American NAVSTAR–GPS and the Russian GLONASS. Within this decade the European system, Galileo, should be operational in the same altitude range, dubbed MEO, Medium Earth Orbit. In this paper the fragmentation of a spacecraft related to one of these three constellations has been simulated and the collision risk faced by the operational satellites has been analyzed. Both the intra-constellation and the inter-constellation risk have been studied. An improvement in the collision risk calculation method developed in (Valsecchi *et al.*, *Space Debris*, 2000) is described in the paper. The new method overcomes the limitation in the application of Öpik's theory of planetary encounters, dictated by the assumption of random orientation of the argument of perigee and the longitude of node of the projectiles, and allows its application to the Medium Earth orbital regime. In general terms it has been observed the the flux following a generic fragmentation is by far larger than the low background flux in MEO. The strong interrelation of the three constellations has been shown by analyzing the inter-constellation effects of the fragmentations. In particular the GPS and the GLONASS are strongly interacting, while the Galileo constellation, orbiting at somewhat higher altitude, is less affected by any unfortunate event happening in the two lower constellations.

INTRODUCTION

Satellite global positioning systems have been deployed in the early 90's as military support systems by the US and the former Soviet Union. Later on, the global positioning systems first became available for private use in 1995, providing an extremely accurate and valuable tool, nowadays used by a huge number of people for many different applications. The satellite positioning systems presently in space are the American NAVSTAR-GPS (Navigation System with Time and Ranging – Global Positioning System) and the Russian GLONASS (Globaluaya Navigatsionnaya Sputnikovaya Sistema).

*ISTI–CNR, Via Moruzzi, 1, 56124 Pisa, Italy
†IASFC–CNR, Via Fosso del Cavaliere 100, 00133 Roma, Italy
‡Telespazio S.p.A., Via Tiburtina 965, 00156 Roma, Italy

	a [km]	e	i [deg]	Number of satellites	Number of planes
Galileo	29994	0	56	30	3
GPS II	26559	0	55	28	6
GLONASS	25478	0	64.8	24	3

Tabella 1: Characteristics of the present and foreseen navigation constellations. Note that the number of satellites include in-orbit spares.

On March 26, 2002 the European Union Transport Ministers gave the final go-ahead on the Galileo project. Galileo, developed by the European Space Agency in collaboration with the European Union, is a civil system, designed to be operational from 2008. Galileo is a 27 satellite Walker constellation (3 planes with 9 satellites each) plus 3 active in-orbit spares, at an altitude of about 23 600 km, with an inclination of 56°. The goal of the Galileo project is to provide Europe, and in general the world, with an accurate, secure and certified satellite positioning system. Galileo should be inter-operable with the existing satellite navigation systems and particularly with the GPS. One of the most ambitious goals of the future satellite systems is, for example, the automatic guidance and control of commercial aircraft. Such an application would of course require an extreme level of reliability.
As seen from Table 1, the Galileo constellation will orbit a region of space (dubbed MEO, Medium Earth Orbit) close to the other two navigation constellations presently deployed. Although the nominal orbits of the different constellations are well separated in altitude, there is the possibility that old uncontrolled spacecraft could intersect the operational orbits. Moreover, although not nearly so crowded as the Low Earth Orbit (LEO), also the MEO region is populated by a large number of space debris. The European Space Agency (ESA) debris environment model[1], MASTER 2001, includes about 60 000 objects larger than 1 cm with orbital elements that are possibly crossing the orbits of the navigation constellations. Actually most of the objects in MEO are clustered about the Molnyia orbits (i.e. with $a \approx 26\,500$, $e \approx 0.7$ and $i \approx 63°$). As a matter of fact these objects have a minimal interaction with the navigation constellations. But, even if we exclude the objects close to Molnyia orbits, about 16 000 objects with diameter larger than 1 cm have orbits potentially crossing the navigation constellations. Figure 1 shows the orbital distribution of this population of objects. Note how, in the lowest panel in Figure 1, the GPS orbit appears within reach of several thousand objects, due to the non-zero eccentricity of most of the debris in the MEO zone. Although lower than in LEO, the average collision velocity at the GPS/GLONASS altitude is still about 5 km/s. At this velocity, an impacting particle of about 1 cm in diameter (corresponding to about 1.5 g) delivers an energy of the order of 10^4 J and is capable of producing severe damages to a spacecraft.

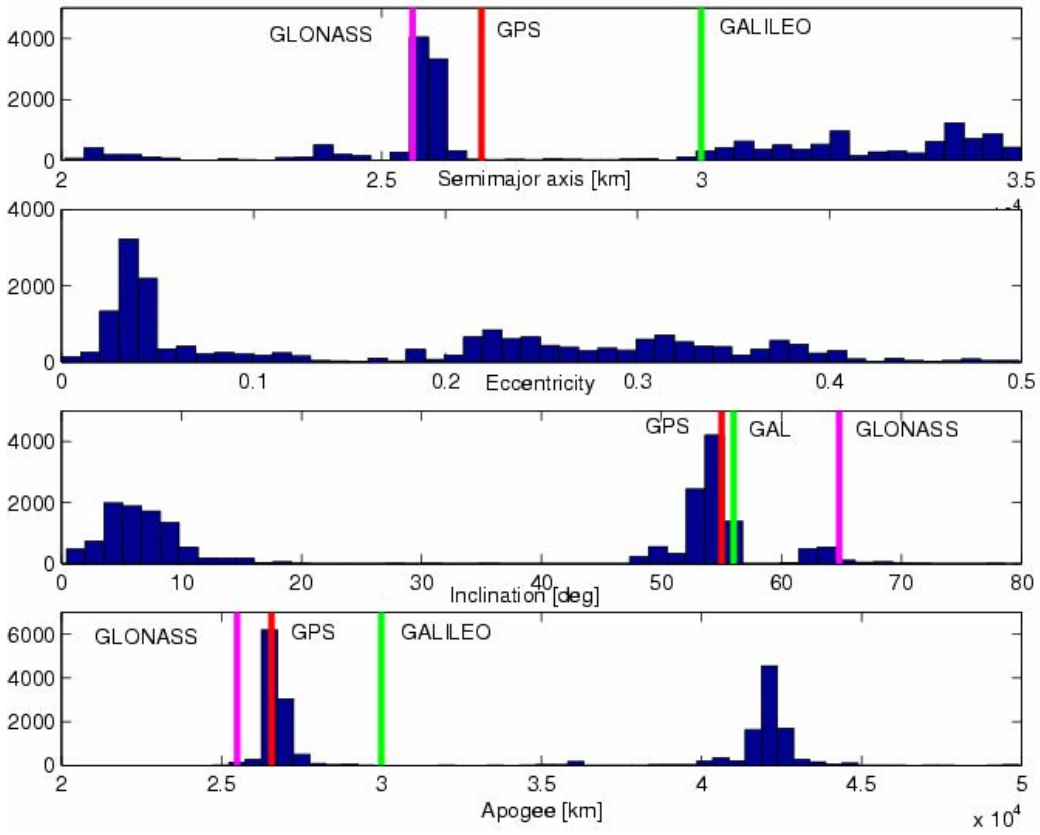

Figura 1: Distribution of the objects with diameters larger than 1 cm in MEO, from the ESA's debris model MASTER 2001. The semimajor axis, eccentricity, inclination and apogee of the objects is shown. The values of the semimajor axis and of the inclination of the GPS, GLONASS and GALILEO orbits is also shown for reference. Note that a cutoff at an eccentricity of 0.5 has been used to exclude all the objects close to Molnyia type orbits.

The sensible applications of the navigation constellations and the absence of any natural sink mechanism (such as the atmospheric drag in LEO) led the GPS operators to the adoption of a debris prevention policy. In particular, as proposed for the geostationary ring, the GPS satellites are moved to a disposal region, about 500 km above the operational orbit, at the end-of-life. Spent upper stages of evolved expandable launch vehicles (EELVs) may also be placed in the disposal region after the completion of their mission. This procedure should prevent any accidental collision between operational satellites and old spacecraft. The disposal zone is in principle well separated both from the GPS operational orbit and from the Galileo planned orbit. Unfortunately the picture is more complicated. In a number of recent papers[2,3] the instability of the GPS disposal orbit, with an increase of the eccentricity that could lead to dangerous crossings of the operational orbits, has been clearly shown. The same is true for the GLONASS related spacecraft.
It is therefore apparent that in a debris mitigation policy the MEO region must be

viewed as a whole and that any action undertaken in a constellation should take into account the presence of the other analogous systems in the vicinity. To further explore the concept of the interdependence of the navigation constellations, in this paper a particularly dangerous situation will be analyzed. The fragmentation of a spacecraft related to one of the navigation constellation (following an explosion or an accidental collision) is simulated. Then the interaction of the debris produced by the fragmentation event with the three constellations is studied. In the next Section the method developed for this analysis will be outlined. Then, in the following Section, the results of the collision risk analysis will be showed and discussed.

COLLISION RISK CALCULATION

Öpik's theory of planetary encounters[4] can be used to analytically calculate the magnitude and direction of the relative velocity vector at impact of a projectile on a given target on circular orbit. Making use of this theory, we developed a method to assess the collision risk for an Earth orbiting satellite. The method is described in Refs. 5 and 6. Here the fundamentals of the method will be briefly recalled.
Let a and e be the semimajor axis and eccentricity of the orbit of the projectile, and I its inclination with respect to the plane of the orbit of the target; the latter, in turn, is on a circular orbit of radius a_0. The velocity U at which the projectile encounters the target is

$$U = \sqrt{\frac{Gm_\oplus}{a_0}} \cdot \sqrt{3 - \frac{a_0}{a} - 2\sqrt{\frac{a(1-e^2)}{a_0}}\cos I}\,,$$

and its component U_r along the direction from the center of the Earth to the target is

$$U_r = \pm\sqrt{\frac{Gm_\oplus}{a_0}} \cdot \sqrt{2 - \frac{a_0}{a} - \frac{a(1-e^2)}{a_0}}\,,$$

where G is the constant of gravity and $m_\oplus$ is the mass of the Earth.
Then, Öpik's expression for the intrinsic collision probability p *per revolution of the projectile*[4] is given by:

$$p_{rev} = \frac{U}{\pi |U_r| \sin I}\,, \tag{1}$$

while the intrinsic probability *per unit time* is obtained by dividing for the orbital period of the projectile:

$$p = \frac{\sqrt{Gm_\oplus}}{2\pi a^{1.5}} \cdot \frac{U}{\pi |U_r| \sin I}\,.$$

Thus, given a target orbit, p is only a function of the orbital elements (a, e and I) of the projectile.
Öpik's theory makes basic assumptions that pose some caveats for its practical application. In particular, it assumes that the argument of perigee ω and the longitude of node Ω of the projectile orbit, evaluated using as reference plane the orbital plane

of the target, are randomly distributed between 0 and 2π. This means, for instance, that the theory is not applicable to situations in which a resonance is constraining the distribution of ω, as is the case, for example, of the Molnyia orbits. These orbits lie at the critical *equatorial* inclination of $i_{eq} = 63°$, and have the *equatorial* argument of perigee constrained in the Southern hemisphere, in order to be high above the horizon for the users located in the former Soviet Union countries; thus, for Molnyia projectiles aimed at a target on circular orbit in the equatorial plane, Öpik's theory would clearly not be applicable. Nonetheless, in LEO, the randomization induced by the drift of ω_{eq} and Ω_{eq} due to the Earth's quadrupole J_2 is so effective that Öpik's theory can be easily applied without significant loss of accuracy[5,6].
On the other hand, the precession rates $\dot{\omega}_{eq}$ and $\dot{\Omega}_{eq}$ are about two orders of magnitude smaller at the GPS altitude than in LEO; in particular, we have $\dot{\Omega}_{eq} \simeq -0.042$ deg/day and $\dot{\omega}_{eq} \simeq -0.02$ deg/day at the GPS altitude. This slower evolution prevents the direct application of our original method to MEOs; we therefore devised an extension to the method presented in Refs. 5 and 6 to take into account also orbital regimes where the randomization of the angular elements cannot be granted, along a line of reasoning similar to that of Ref. 7.
Let us discuss the reasoning that is at the basis of the assumption of a flat distribution in Ω and ω in the derivation of Eq. (1). Necessary conditions for a collision to occur are:

- that the perigee and apogee of the projectile orbit are such that $q = a(1-e) < a_0 < Q = a(1+e)$;
- that the geocentric distance of the projectile, at its crossings of the orbital plane of the target, be equal to a_0.

These crossings take place at the ascending and the descending nodes of the projectile orbit on the target orbital plane, where we have $\omega + f = 0$ (at the ascending node, f being the true anomaly of the projectile), and $\omega + f = 180°$ (at the descending node); the geocentric distances of the nodal points are given by

$$\begin{aligned} r_a &= \frac{a(1-e^2)}{1+e\cos(-\omega)} = \frac{a(1-e^2)}{1+e\cos\omega} \\ r_d &= \frac{a(1-e^2)}{1+e\cos(180°-\omega)} = \frac{a(1-e^2)}{1-e\cos\omega}\,. \end{aligned}$$

When both r_a and r_d are sufficiently different from a_0, collisions are impossible; this happens most of the time during the perturbation-induced rotation ω, but sooner or later, unless a specific dynamical mechanism limits the range of values attainable by ω, it will happen that, for a particular value ω_c of ω,

$$a_0 = \frac{a(1-e^2)}{1+e\cos\omega_c}\,.$$

This collision condition is, in general, not alone; in fact a collision is also possible for $\omega_c + 180°$, i.e. at the other node, as discussed above. Moreover, taking into account

that, for any angle α, $\cos\alpha = \cos(360^\circ - \alpha)$, collisions will also be possible for $360 - \omega_c$ and for $180 - \omega_c$. It is easy to check that these four values of ω are all in different quadrants: let us call ω_{c1} the one in the first quadrant, then $\omega_{c4} = 360^\circ - \omega_{c1}$ is in the fourth, while $\omega_{c3} = \omega_{c1} + 180^\circ$ and $\omega_{c2} = 180 - \omega_{c1}$ are, respectively, in the third and in the second quadrant.
The derivation of Öpik's expression (Eq.(1)) consists in a particle-in-the-box evaluation of the probability of presence of the projectile in a solid ring of radius a_0, with very small horizontal and vertical thickness; in this context, the assumption of the randomness of ω allows the explicit computation of the probability of presence of the projectile in the ring. If the probability distribution of the argument of perigee of the projectile orbits is not flat, we need a way to take this into account by appropriately rescaling the probability of presence of the projectile in the above described ring.
Let us introduce the quantity

$$\omega^\star = \min(\omega - \omega_{c1}, \omega - \omega_{c2}, \omega - \omega_{c3}, \omega - \omega_{c4});$$

it is a simple function that expresses the difference between the current value of ω and the nearest collision solution.
The ω-randomness assumption of Öpik's theory can be considered equivalent to the assumption that the distribution of $\omega^\star$ is flat between -180° and 180°; in particular, this means that, given a population consisting of N projectiles, Öpik's assumption implies that there should be

$$y_f = \frac{N\delta\omega^\star}{2\pi}$$

projectiles in a small interval of width $\delta\omega^\star$ centered on $\omega^\star = 0$.
On the other hand, it is easy to compute the true distribution of $\omega^\star$ for all the projectiles (from the results of the numerical integration of the orbit of the debris cloud). We can then compare at any given instant in time, as in Figure 2, the value of the true distribution of the $\omega^\star$ at 0°, y_t, with the value of the flat distribution, y_f. Then, the ratio y_t/y_f gives the correction factor by which the probability of collision, given by Eq. (1), calculated assuming the flat distribution of perigee arguments, has to be multiplied. In this way, for each projectile, the true collision probability, taking into account the slow diffusion of the orbital elements in MEO, is obtained.
The remaining open question is a procedure to compute ω, the argument of perigee of the projectile computed with respect to the orbital plane of the target; this is dealt with in the following.
Given an orbit with semimajor axis a, eccentricity e, equatorial inclination i_{eq}, equatorial longitude of node Ω_{eq}, and equatorial argument of perigee ω_{eq}, the magnitude of its angular momentum vector $\vec{h}$ is given by[8]:

$$h = \sqrt{Gm_\oplus a(1-e^2)}\,.$$

The vector $\vec{h}$ can be written as $\vec{h} = \vec{i}h_x + \vec{j}h_y + \vec{k}h_z$, where $\vec{i}$, $\vec{j}$ and $\vec{k}$ are orthogonal unit vectors oriented along the usual x-y-z axes (the x and y-axes in the equatorial

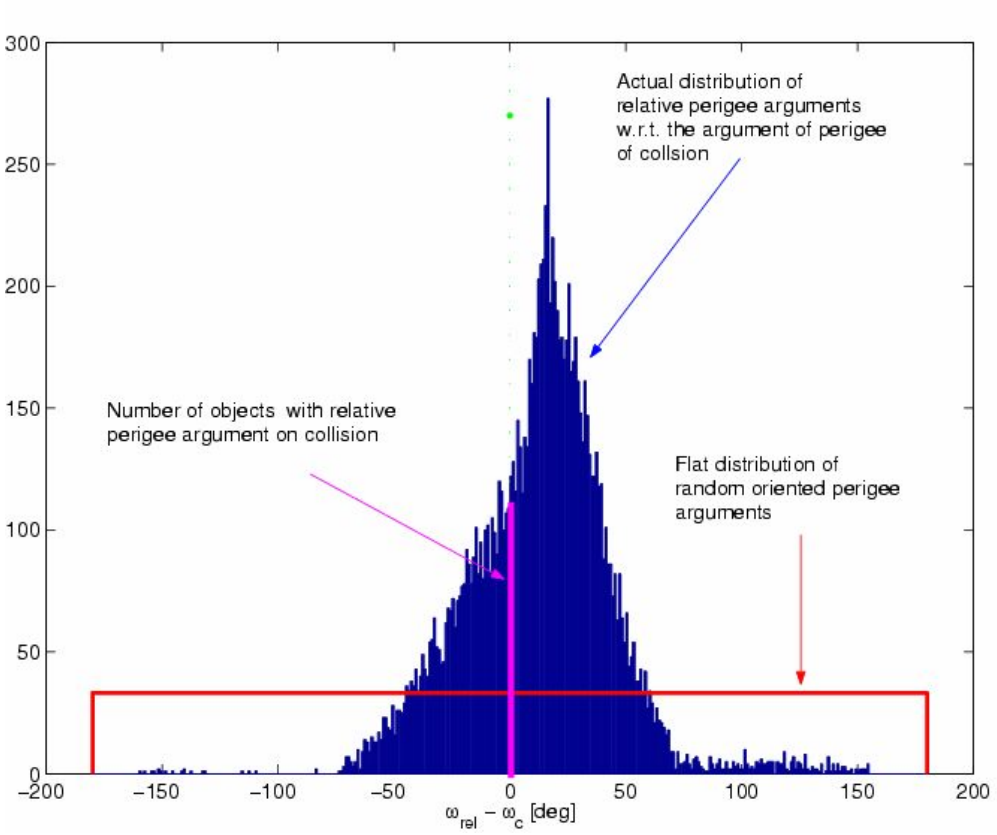

Figura 2: Example of the distribution of the true $\omega^\star$ for a debris cloud generated by an explosion, with respect to a flat distribution of relative arguments of perigee.

plane, the z-axis normal to it, with the x-axis directed toward the γ-point). We have:

$$h_{xy} = \sqrt{h_x^2 + h_y^2} = h \sin i_{eq}$$

$$\begin{aligned} h_x &= h_{xy} \sin \Omega_{eq} = h \sin i_{eq} \sin \Omega_{eq} \\ h_y &= -h_{xy} \cos \Omega_{eq} = -h \sin i_{eq} \cos \Omega_{eq} \\ h_z &= h \cos i_{eq}, \end{aligned} \tag{2}$$

Then, the vector $\vec{\varepsilon} = \vec{i}\varepsilon_x + \vec{j}\varepsilon_y + \vec{k}\varepsilon_z$, is defined as $\vec{\varepsilon} = GM\vec{e}$ where $\vec{e}$ is a vector with the magnitude of the osculating eccentricity drawn from the center of the Earth toward the perigee. The components of $\vec{\varepsilon}$ can be written as:

$$\begin{aligned} \varepsilon_x &= \frac{h_x \varepsilon_y - \varepsilon h_{xy} \cos \omega_{eq}}{h_y} \\ \varepsilon_y &= \frac{\varepsilon h_x \cos \omega_{eq} - \varepsilon_z h_z h_y / h_{xy}}{h_{xy}} \\ \varepsilon_z &= \frac{h_{xy} \varepsilon \sin \omega_{eq}}{h} \end{aligned} \tag{3}$$

so that, by using Eqs. (2) and (3), we can write the unit vectors $\hat{h}$ and $\hat{\varepsilon}$ as:

$$\begin{aligned}\hat{h} &= \begin{pmatrix} \sin i_{eq} \sin \Omega_{eq} \\ -\sin i_{eq} \cos \Omega_{eq} \\ \cos i_{eq} \end{pmatrix} \\ \hat{\varepsilon} &= \begin{pmatrix} \cos \omega_{eq} \cos \Omega_{eq} - \cos i_{eq} \sin \omega_{eq} \sin \Omega_{eq} \\ \cos \omega_{eq} \sin \Omega_{eq} + \cos i_{eq} \sin \omega_{eq} \cos \Omega_{eq} \\ \sin i_{eq} \sin \omega_{eq} \end{pmatrix}. \end{aligned} \tag{4}$$

Suppose we now have two sets of orbital elements, one relative to the target $(a_0, e_0, i_{0eq}, \omega_{0eq}, \Omega_{0eq})$, and the other relative to the projectile $(a, e, i, \omega_{eq}, \Omega_{eq})$.
We want to compute the inclination, I and the argument of perigee, ω of the projectile in a reference frame X-Y-Z, in which the orbit of the target has inclination equal to zero, and the X-axis is directed along the nodal line, on the equator, of the target orbit. To obtain I, we just have to compute:

$$\begin{aligned}\cos I &= \hat{h} \cdot \hat{h}_0 \\ &= \sin i_{eq} \sin i_{0eq} (\sin \Omega_{eq} \sin \Omega_{0eq} + \cos \Omega_{eq} \cos \Omega_{0eq}) + \cos i_{eq} \cos i_{0eq}. \end{aligned} \tag{5}$$

To compute ω, we apply a rotation of $-\Omega_{0eq}$ about the z-axis (given by the rotation matrix $R_{-\Omega_0}$); after this rotation the old x-axis has been transformed into the new X-axis, directed along the nodal line, on the equator, of the target orbit. We then apply a rotation of $-i_{0eq}$ about the X-axis (given by the rotation matrix R_{-i_0}). The rotation of the unit vectors of the target orbit, from Eq. (4), is given by:

$$\begin{aligned}\hat{h}_{0r} &= R_{-i_0} R_{-\Omega_0} \hat{h}_0 = \begin{pmatrix} 0 \\ 0 \\ 1 \end{pmatrix} \\ \hat{\varepsilon}_{0r} &= R_{-i_0} R_{-\Omega_0} \hat{\varepsilon}_0 = \begin{pmatrix} \cos \omega_{0eq} \\ \sin \omega_{0eq} \\ 0 \end{pmatrix}. \end{aligned}$$

For the projectile orbit we have analogously:

$$\begin{aligned}\hat{h}_r &= R_{-i_0} R_{-\Omega_0} \hat{h} \\ &= \begin{pmatrix} \sin i_{eq} (\sin \Omega_{eq} \cos \Omega_{0eq} - \cos \Omega_{eq} \sin \Omega_{0eq}) \\ -\sin i_{eq} \cos i_{0eq} (\sin \Omega_{eq} \sin \Omega_{0eq} + \cos \Omega_{eq} \cos \Omega_{0eq}) + \cos i_{eq} \sin i_{0eq} \\ \sin i_{eq} \sin i_{0eq} (\sin \Omega_{eq} \sin \Omega_{0eq} + \cos \Omega_{eq} \cos \Omega_{0eq}) + \cos i_{eq} \cos i_{0eq} \end{pmatrix} \end{aligned}$$

and

$$\hat{\varepsilon}_r = R_{-i_0} R_{-\Omega_0} \hat{\varepsilon}\,.$$

By substituting Eq. (4), and developing, we obtain the rotated unit vectors of $\hat{\varepsilon}_r$ as:

$$\begin{aligned}
\hat{\varepsilon}_{xr} &= \cos\omega_{eq}(\cos\Omega_{eq}\cos\Omega_{0eq} + \sin\Omega_{eq}\sin\Omega_{0eq}) \\
&\quad + \cos i_{eq}\sin\omega_{eq}(\cos\Omega_{eq}\sin\Omega_{0eq} - \sin\Omega_{eq}\cos\Omega_{0eq}) \\
\hat{\varepsilon}_{yr} &= \sin\omega_{eq}[\sin i_{eq}\sin i_{0eq} + \cos i_{eq}\cos i_{0eq}(\cos\Omega_{eq}\cos\Omega_{0eq} + \sin\Omega_{eq}\sin\Omega_{0eq})] \\
&\quad - \cos\omega_{eq}\cos i_{0eq}(\cos\Omega_{eq}\sin\Omega_{0eq} - \sin\Omega_{eq}\cos\Omega_{0eq}) \\
\hat{\varepsilon}_{zr} &= \sin\omega_{eq}[\sin i_{eq}\cos i_{0eq} - \cos i_{eq}\sin i_{0eq}(\cos\Omega_{eq}\cos\Omega_{0eq} + \sin\Omega_{eq}\sin\Omega_{0eq})] \\
&\quad + \cos\omega_{eq}\sin i_{0eq}(\cos\Omega_{eq}\sin\Omega_{0eq} - \sin\Omega_{eq}\cos\Omega_{0eq})\,.
\end{aligned}$$

Finally, from Eqs. (3), we have:

$$\cos\omega = \frac{\hat{\epsilon}_{yr}\hat{h}_{xr} - \hat{\epsilon}_{xr}\hat{h}_{yr}}{\hat{h}_{xyr}} \tag{6}$$

$$\sin\omega = \frac{\hat{\varepsilon}_{zr}}{\hat{h}_{xyr}}\,. \tag{7}$$

With Eqs. (5), (6), and (7) it is possible to completely describe the dynamics of the debris cloud with respect to the target orbit. In the next Section the results of the application of this improved method to the Navigation Constellations are shown.

DESCRIPTION OF THE SIMULATIONS

In Refs. 6, 9 and 10 the hazard posed to a LEO multi-plane constellation by the fragmentation of a spacecraft inside the constellation itself has been analyzed. It has been shown that the interaction of the evolving debris orbits with the global dynamics of the system gives way to a long lasting collision flux exceeding the background debris flux for long interval of times after the event. It has also been shown how the effects are different on the various constellation planes, according to the plane in which the fragmentation takes place.

Exploiting the advancements in the collision probability calculation method described in the previous Section, in this paper a similar study is performed for the MEO navigation constellations. In particular a number of tests have been performed, simulating the fragmentation either of a Galileo or of a GPS or of a GLONASS related spacecraft. Both an explosion induced or a collision induced break-up have been studied. In Table 2 the type of event, the orbital elements and the mass of the parent spacecraft and the number of debris larger than 1 cm produced by the fragmentation, are given. In the simulation process the fragments down to 1 mg are produced, but only those with diameters larger than 1 cm (corresponding to about 1.5 g) are considered. In Table 2 it can be noted that the first two simulated fragmentations pertain to spacecraft in Galileo-like orbits, the next two events are related to spacecraft in GPS-like orbits and the last two fragmentations relate to spacecraft in GLONASS-like orbits. The planes of the fragmentation events are taken as "reference" planes (i.e., plane number 1) for the corresponding constellations, in the following analysis. Note that in all the simulated collision events the mass and the velocity of the

Type of event	a [km]	e	i [deg]	Ω [deg]	ω [deg]	Mass of the spacecraft [kg]	Number of debris larger than 1 cm
Explosion	29994	1×10^{-3}	56.0	262.7	56.9	2000	72 100
Collision	29994	1×10^{-3}	56.0	262.7	56.9	2000	18 300
Explosion	26559.74	0	55.0	274.0	50.0	922	33 200
Collision	26559.74	0	55.0	274.0	50.0	2339	14 000
Explosion	25478	1×10^{-3}	64.7	262.7	56.9	2121	76 200
Collision	25478	1×10^{-3}	64.7	262.7	56.9	2121	16 800

Tabella 2: Characteristics of the simulated fragmentation events.

projectile were set to 10 kg and 5 km/s, respectively. With these values the specific energy for catastrophic break-up, i.e. the ratio between the projectile energy and the target mass, is larger than the threshold discriminating between a localized, crater-like, target damage and a total fragmentation. Therefore the targets are fragmented. The mass distribution of these fragments is a power law with an energy-dependent exponent[11] and the velocity increment ΔV of the fragments as a function of size is obtained extracting from a triangular distribution with the peak value given by the "intermediate" model proposed in Ref. 12. In the explosion cases, a high intensity explosion according to the model described in Ref.11 is simulated. Then the orbit of the fragments larger than 100 g is individually propagated, for 20 years, taking into account all the main gravitational and non-gravitational perturbations (Earth geopotential harmonics, luni-solar perturbations, air drag and solar radiation pressure). The smaller fragments are sampled, with a sampling factor of 5. The orbit of the constellation satellites is propagated, again for 20 years, by taking into account only the J_2 perturbations, to simulate the station keeping of the controlled operative satellites.

Considering all the fragments produced by the simulated fragmentation event, the total projectile flux as a function of altitude and mass is computed, with the method described in the previous Section, by adding up the contributions of all the fragments for which an impact becomes possible. Then the flux of the simulated collision fragments is compared, for any given range of projectile energies, to the reference value corresponding to the background flux resulting from the entire debris population currently present in space. The background flux is estimated by the SDM[11] code, using the MASTER 2001 population of orbital debris. The difference between these two fluxes will give a clear estimate of the extra collision risk faced by the constellation satellites due to the consequences of the simulated break-up.

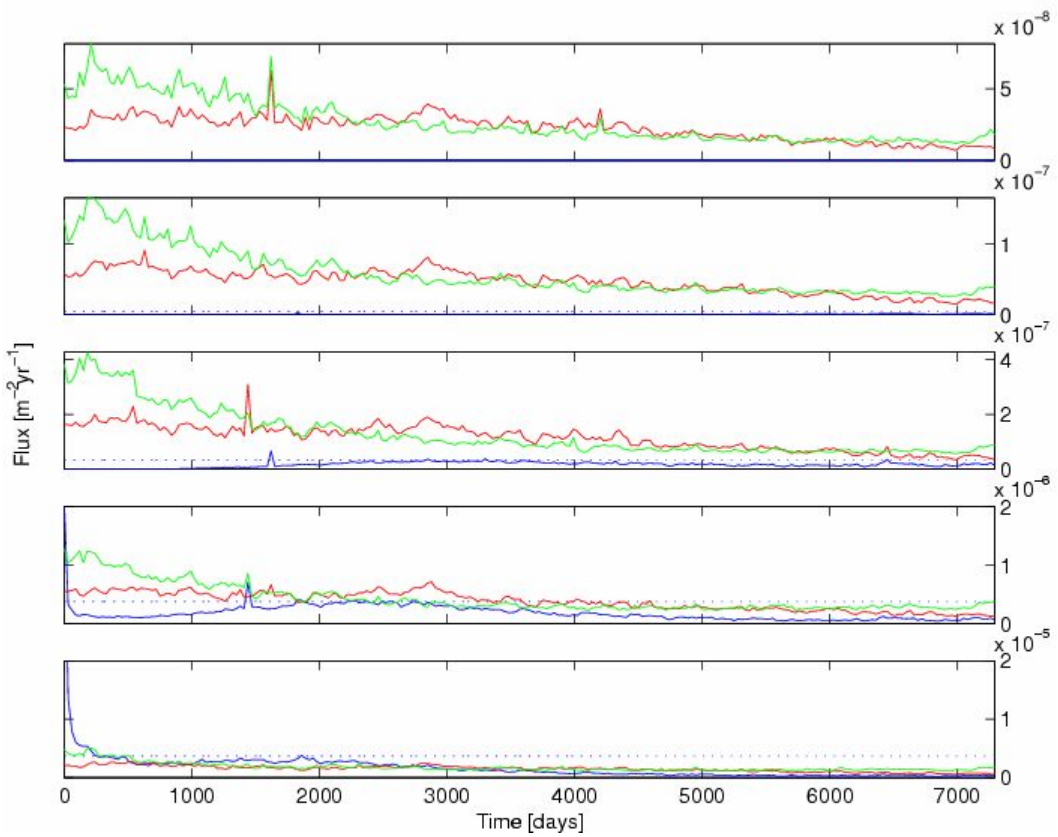

Figura 3: Flux of fragments vs. time, on the three Galileo constellation planes, produced by a simulated explosion of a spacecraft on a constellation plane. Each curve represents the flux affecting one of the three constellation planes. The five panels show, from bottom to top, the fluxes at increasing impact energies E: $10^3 < 2E < 10^4$ J; $10^4 < 2E < 10^5$ J; $10^5 < 2E < 10^6$ J; $10^6 < 2E < 10^7$ J; $10^7 < 2E < 10^8$ J. The horizontal dotted lines represent the background fluxes in the same energy ranges, computed from the overall space debris population included in MASTER 2001.

RESULTS

The effect of the fragmentations described in Table 2 have been analyzed in terms of flux of particles on the different planes of a constellation. Both the intra-constellation and the inter-constellation effects have been studied. This means that, e.g., an explosion of a spacecraft in a Galileo-like orbit has been studied with respect both to the Galileo constellation itself and with respect to the GPS constellation. Figure 3 shows the flux of debris, in m^{-2} yr^{-1}, coming from the first explosion of Table 2, on the three planes of the Galileo constellation (i.e., including the plane of the fragmentation itself). In every panel, each one of the three curves shows the flux with respect to one of the planes; in particular, looking at the bottom panel, the curve starting from the highest flux value and then rapidly decreasing, represents the flux on the same

explosion plane. This flux of low energetic particles is composed by a large number of debris that, just after the fragmentation event, remain clustered around the parent body orbit. The small relative inclination between the target plane and the debris orbits account for low impact velocities, hence for the low energy of the impact. In the same panel the two lower, almost overlapping, curves represent the flux on the planes with nodes shifted by 120° (lowest curve) and 240° (intermediate curve) from the explosion plane. In the second panel from bottom, corresponding to the interval $10^4 < 2E < 10^5$ J in impact energy, in the very first days the curve relative to the flux on the same explosion plane is the highest one, although rapidly declining. After this short transient, the top curve becomes the one related to the plane at 240° from the explosion. The curve of the flux on the plane at 120° becomes the intermediate one. In the upper panels, the flux of more energetic particles on the same plane of the explosion is negligible (again due to the low relative inclination, very slowly evolving due to the slow relative nodal regression). The curves of the flux on the other two planes are again in the same order an in the previous panel. The small number of well separated planes and, especially, the slower dynamics of MEO account for a global behavior different from the one shown in Refs. 6, 9 and 10 for the LEO constellations. As expected, the fluxes of debris are about two orders of magnitude lower than the fluxes registered in the case of a LEO IRIDIUM-like constellation (see, e.g., Figure 6 in Ref. 6), mainly due to the lower orbital velocity and relative inclinations. It has however to be noted how, in the top three panels, the fluxes of explosion debris on the planes shifted from the explosion one, are several times larger than the background flux. It is worth stressing that the higher panels correspond to impact energies that can severely damage a spacecraft and that, in the top panel, the range of energy between 10^7 and 10^8 J, is of the order of the fragmentation threshold for a Galileo satellite. Nonetheless it must also be remembered that the flux levels are quite low and account for a hazard of damaging impacts of the order of 10^{-3} – 10^{-4} over a decade.

In Figure 4 the flux, on the three planes of the Galileo constellation, of the debris produced by a collisional break-up of a spacecraft in a Galileo-like orbit is shown. The five lowest panels correspond to the five panels of Figure 3. These panels display a behavior similar to those of the explosion case. The main difference with respect to Figure 3 is the presence of the two additional panels covering the highest ranges of energy. This is due to the presence, in the mass distribution of the collision events, of a small number of large fragments capable of delivering these higher impact energy to the target. Nonetheless, the resulting fluxes are very low due to the low number of fragments involved.

The situation becomes more involved in the case of the GPS constellation (Figure 5). The presence of six orbital planes, spaced by only 60°, makes the picture closer to the one observed in the LEO constellations. As in Figure 3, in the two lowermost panels of Figure 5, after a short interval following the fragmentation, the flux of debris on the same plane of the explosion falls abruptly. In the same panels, the flux on the other four planes is comparable, with the planes from 60° to 180° apart experiencing

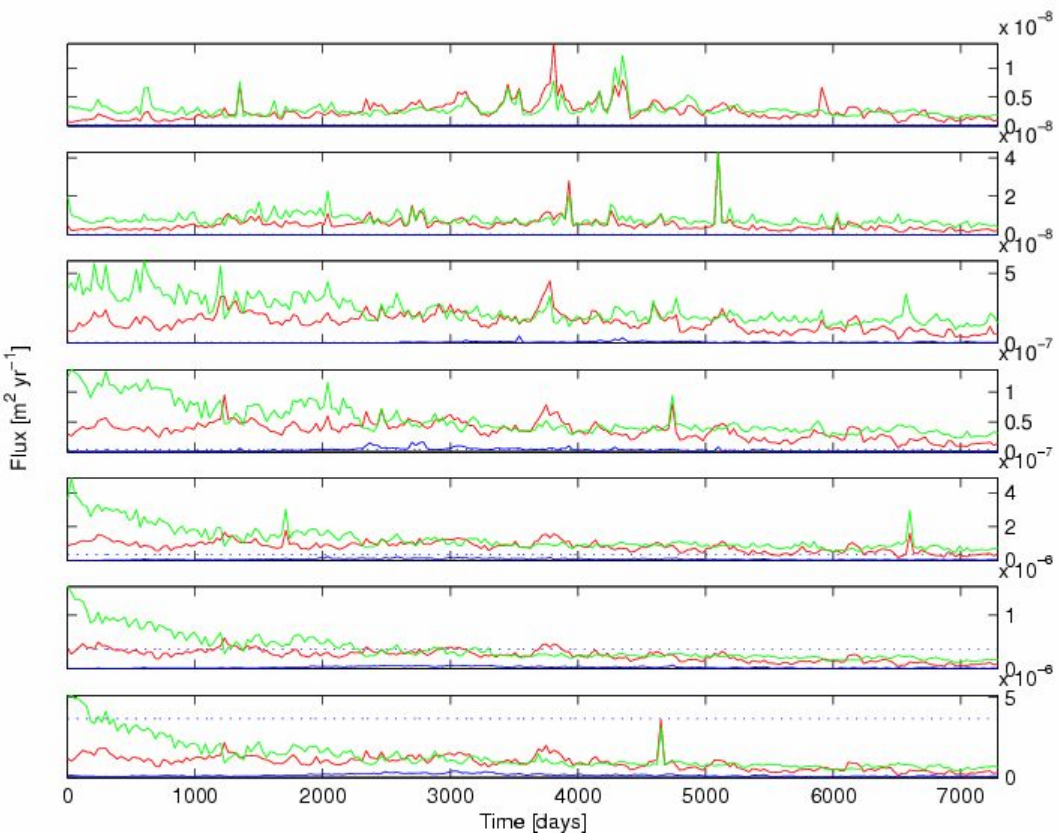

Figura 4: The same as Figure 3 for the case of a collisional break-up of a spacecraft in a Galileo-like orbit. The seven panels show, from bottom to top, the fluxes at increasing impact energies E: $10^3 < 2E < 10^4$ J; $10^4 < 2E < 10^5$ J; $10^5 < 2E < 10^6$ J; $10^6 < 2E < 10^7$ J; $10^7 < 2E < 10^8$ J, $10^8 < 2E < 10^9$ J; $2E > 10^9$ J.

the highest values several years after the explosion. In the three upper panels the effect of the differential precession of the orbital nodes becomes more apparent (as it was in LEO) and the fluxes rise at successive times, according to the nodal separation with respect to the event plane. In particular, in the second panel from top, it can be noted, starting from about 1500 days after the explosion, a first rise of the line related to the plane at 60°, followed by all the others until the one at 240° apart, that start to rise at about 4500 days. Only the flux on the plane 300° apart does not display a significant enhancement during the simulation time span. By the time this plane should be reached by the drifting projectile nodes, the cloud is already quite dispersed. The values of the fluxes are similar to those observed in Figure 3. The background values are instead higher at the GPS altitude. This is due to the fact that presently no constellation is actually deployed at the Galileo altitude. Nonetheless, also for the GPS case, the explosion debris flux is, for several years, a few times higher than the background in all the energy ranges.
In the case of a collision on a GPS-like orbit the situation is similar to the explosion

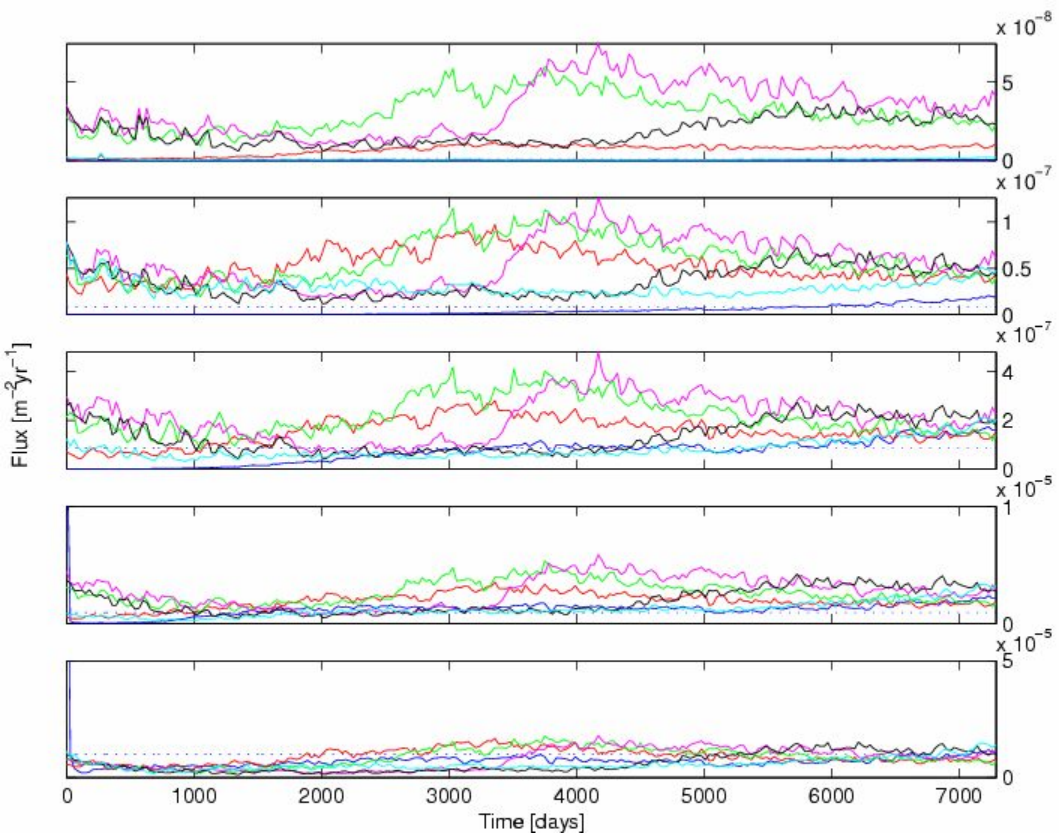

Figura 5: The same as Figure 3 for the case of the explosion of a spacecraft in a GPS-like orbit.

one. The main difference is again that also the highest energy intervals become populated, as in Figure 4. The cases related to events in a GLONASS-like orbit display behaviors comparable to the Galileo constellation and are therefore not shown.

The next step was to analyze the effect of a fragmentation happening in a given constellation with respect to the other ones. As pointed out before, the proximity of the orbits of the three constellation makes them interdependent. Figure 6 shows the flux, on the three Galileo planes, of the debris coming from the explosion of a spacecraft in a GPS-like orbit. Note that the plane of the exploding spacecraft has $\Omega = 274°$, while the Galileo plane number 1 in Figure 6 is supposed to be at $\Omega = 262.7°$ (the following two planes are, as usual, 120° and 240° apart). In the three lower panels the fluxes on the Galileo planes are comparable, only a few times lower, with those observed in Figure 3. The curve that has a long peak, after about 1500 days from the explosion, represents the flux on the plane shifted by 120°. After this interval of time, due to the evolution of the mutual inclinations, this plane faces almost head-on collisions with the debris that gained enough eccentricity, from the breakup ΔV, to reach Galileo near apogee. In the two upper panels the flux is about one order of magnitude lower than in Figure 3, also for the most exposed plane at

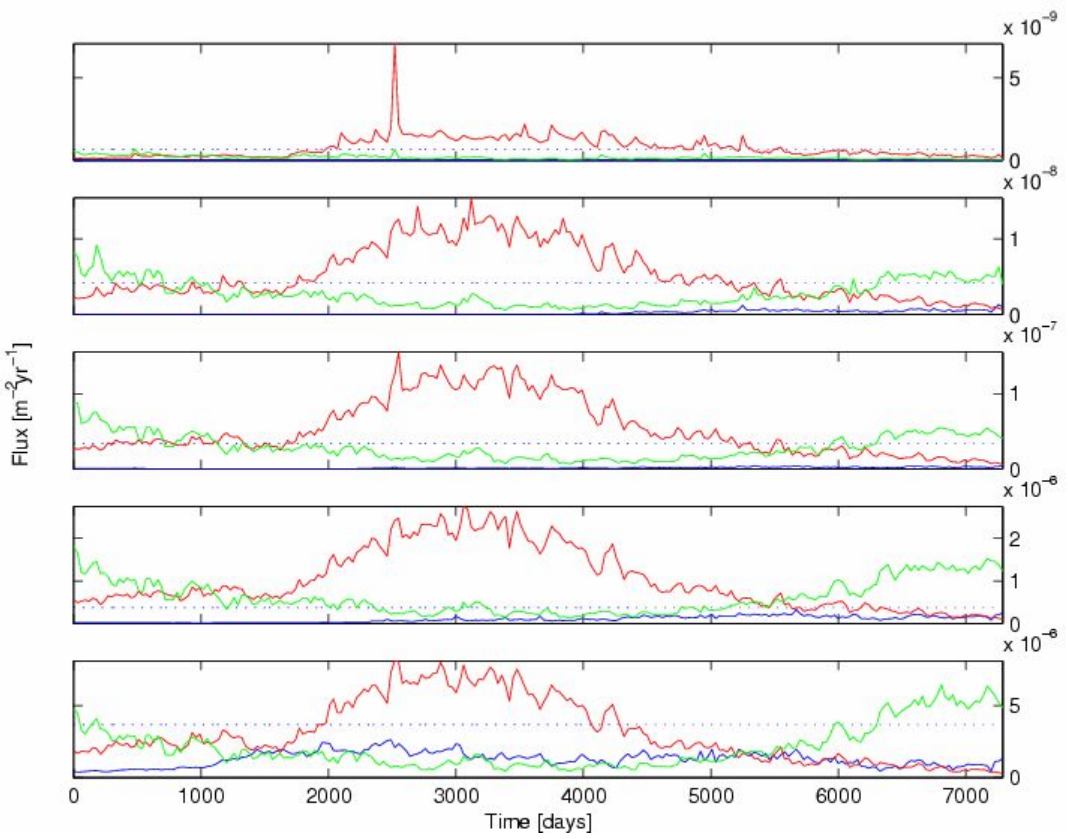

Figura 6: Flux on the Galileo constellation planes due to the debris produced by the explosion of a spacecraft in a GPS-like orbit. The panels are the same as in Figure 3.

120°. This should be due to the fact that heavier debris, capable of delivering the higher impact energies displayed in these panels, do not get enough ΔV to reach the Galileo altitude.

In Figure 7 the opposite situation is shown. The effects, on the GPS constellation, of the explosion of a spacecraft in a Galileo-like orbit are analyzed. The most noticeable feature is that the flux in the energy range $10^5 < 2E < 10^6$ J (third panel) is at the same level of the case of the explosion of a spacecraft in the GPS orbit (Figure 5). In the other panels the fluxes are between one order of magnitude and one half times lower than in Figure 5. In all the panels the highest flux is observed on the plane at 180° from the reference plane. This plane is nearly counter rotating with respect to the plane of the exploding Galileo spacecraft and is therefore subject to high velocity collisions. The second highest flux is then observed, starting from about 900 days after the event, on the plane at 240°, as the mutual inclination evolution brings the plane to interact with the cloud of debris.

Finally the different effect of an explosion of a spacecraft in a GLONASS-like orbit on the Galileo (Figure 8) and the GPS (Figure 9) constellations is analyzed. In Figure 8 it can be noted how the effects on the Galileo constellation are mitigated by

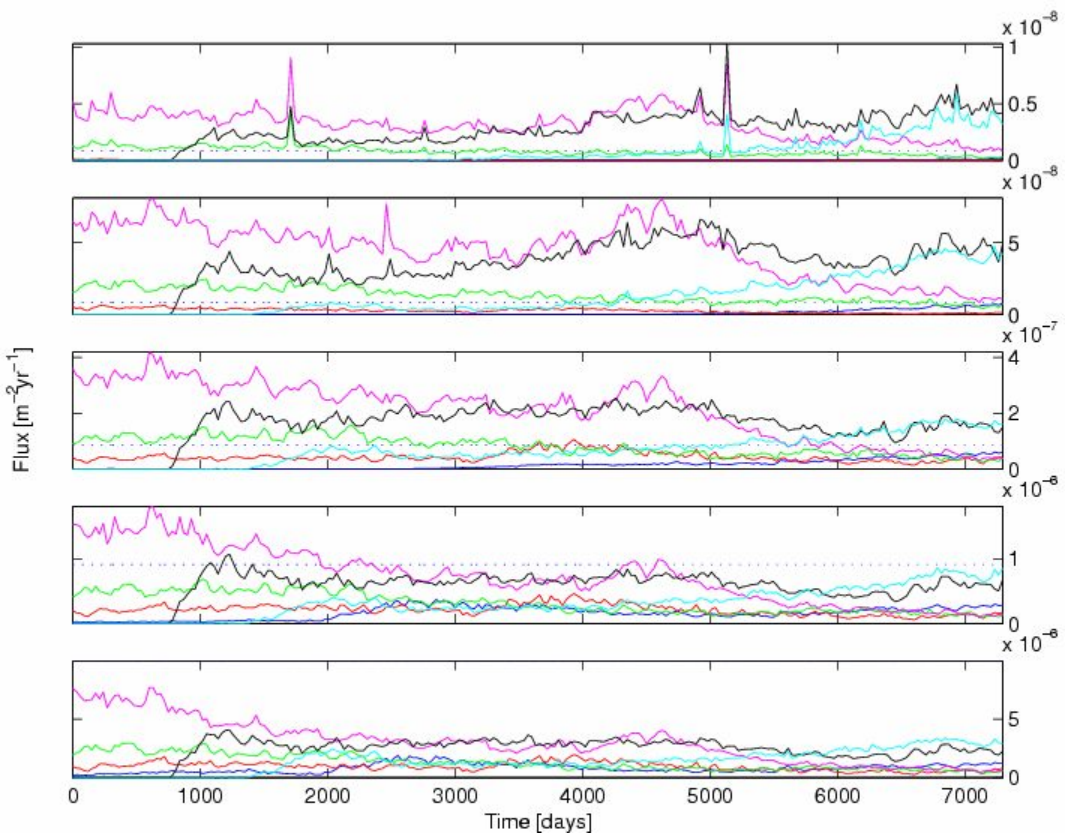

Figura 7: Flux on the GPS constellation planes due to the debris produced by the explosion of a spacecraft in a Galileo-like orbit. The panels are the same as in Figure 3.

the large separation in altitude between this constellation and the GLONASS. Only the flux on the plane shifted by 120° is noticeable. In the four lowest panels this flux is actually comparable to the fluxes of Figure 3. For the upper panel the same considerations as in Figure 6 hold. The other planes appears to be almost not affected at all by the fragmentation debris. The picture becomes quite different if the effects of the GLONASS explosion on the GPS constellation are displayed. In Figure 9 the fluxes on all the GPS planes are generally at least at the same level as in Figure 5. In particular, in the two uppermost panels the fluxes are even about one order of magnitude larger than the corresponding ones in Figure 5. The most exposed planes are again those at 180°, 120° and 240° (in the order in which the curves appear, from top to bottom, in the second panel from top). Due to the comparatively small separation in altitude of the two constellations an increase of eccentricity of less than 5 % makes a debris coming from the GLONASS altitude a possible projectile for a GPS satellite. This increment in eccentricity is easily obtained with the ΔVs of a few hundred m/s due to the explosion.

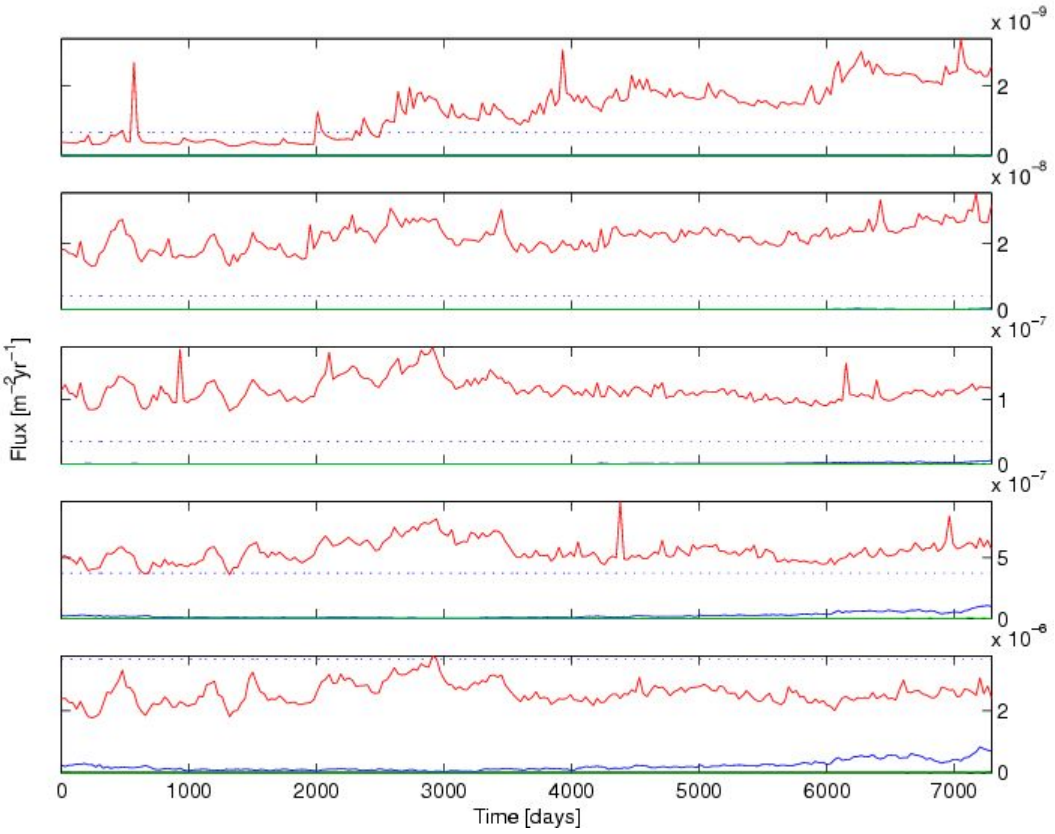

Figura 8: Flux on the Galileo constellation planes due to the debris produced by the explosion of a spacecraft in a GLONASS-like orbit. The panels are the same as in Figure 3.

CONCLUSIONS

Thanks to the improvement of the method described in this paper with respect to the one developed in Refs. 5 and 6, the collision risk for the navigation constellations, following a fragmentation of a spacecraft, has been analyzed. The slower dynamics (in terms of precession of the angular arguments of an orbit) of the MEO region prevent the appearance of the strong global effects observed for the LEO constellations[6,10]. Nonetheless a selection of the incident flux according to the initial location of the fragmentation event with respect to a given plane can still be observed. The planes that have a node displaced by about 180° from the one of the event are generally more exposed to strong incident fluxes. Hence they face a higher risk of a damaging collision. In general terms it has been observed the the flux following a generic fragmentation is by far larger than the low background flux in MEO. The values, spanning the range $10^{-6} \div 10^{-8}$ m^{-2} yr^{-1} according to the different impact energy levels, still account for low risks in terms of impacts per year. However, the very sensible applications of the navigation constellation call for a high level of reliability that could be seriously endangered by such prolonged levels of debris fluxes. Moreover the strong

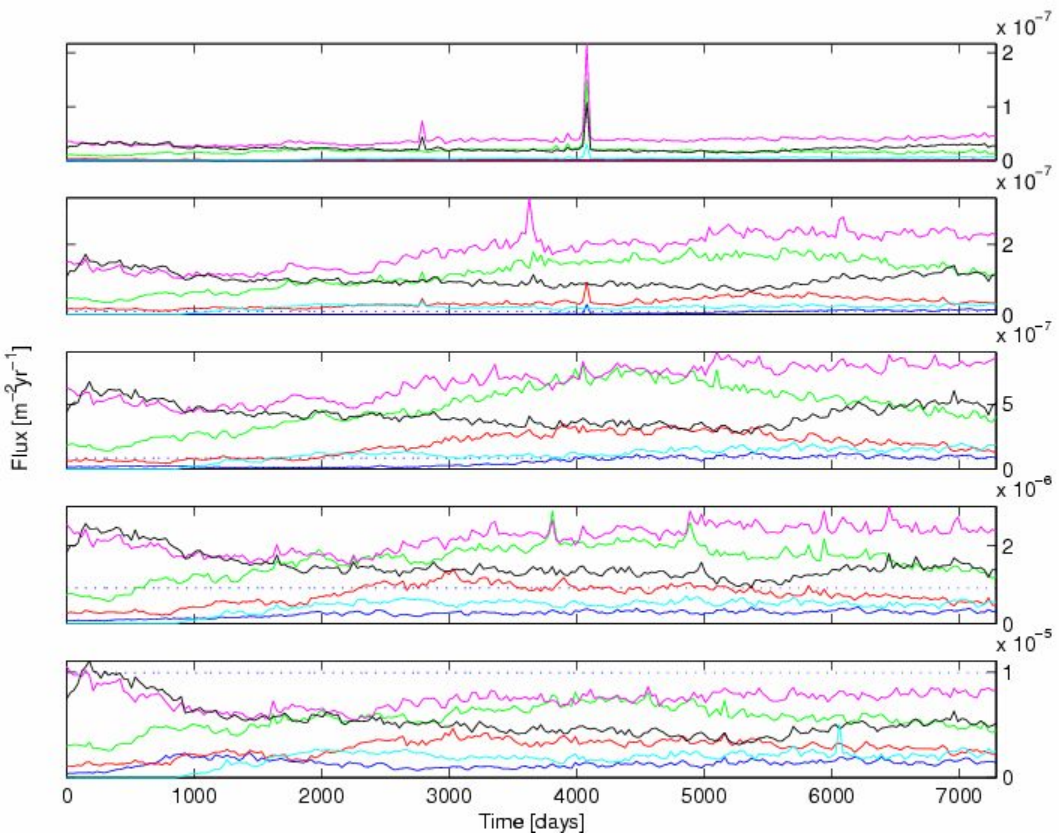

Figura 9: Flux on the GPS constellation planes due to the debris produced by the explosion of a spacecraft in a GLONASS-like orbit. The panels are the same as in Figure 3.

interdependence of the three constellations has been highlighted, by displaying the inter-constellations effects of an explosion event. In some cases the geometry of the systems is such that a larger flux is experienced if the fragmentation event happens on a different constellation. This effect is apparent comparing Figure 5 with Figure 9. On the other hand the results shown by Figure 8 would suggest that an increased separation in altitude could protect the forthcoming Galileo from any unfortunate event happening in the two lower constellations.
Therefore the mitigation policies of the different constellations should be harmonized, viewing the navigation constellation orbital regime as a whole region to be protected against a possible future debris growth.

BIBLIOGRAPHY

1. H. Klinkrad, J. Bendisch, K.D. Bunte, H. Krag, H. Sdunnus and P. Wegener, "The MASTER-99 space debris and meteoroid environment model", *Advances in Space Research*, **28**, 1355-1366, 2001.
2. C.C. Chao and Gick R.A., "Long-term evolution of navigation satellite orbits:

GPS/Glonass/Galileo", paper COSPAR 02-A-02858, *Advances in Space Research*, in press, 2002.
3. A.B. Jenkin and Gick R.A., "Collision risk posed to the Global Positioning System by disposal orbit instability", *Journal of Spacecraft and Rockets*, **39**, No. 4, 532–539, 2002.
4. E.J. Öpik, *Interplanetary Encounters*, Elsevier, New York, USA, 1976.
5. G.B. Valsecchi, A. Rossi and P. Farinella, "Visualizing impact probabilities of space debris", *Space Debris*, **1** (2), pp. 143 – 158, 2000.
6. A. Rossi, G.B. Valsecchi and P. Farinella, "Collision risk for high inclination satellite constellations", *Planetary and Space Science*, **48**, 319–330, 2000.
7. A. Dell'Oro and Paolicchi P., "Statistical properties of encounters among asteroids: a new, general purpose, formalism", *Icarus*, **136**, 328–339, 1998.
8. A.E. Roy, *Orbital motion*, Adam Hilger Ltd., Bristol, UK, 1982.
9. A. Rossi, G.B. Valsecchi and P. Farinella, "Risk of collision for constellation satellites", *Nature*, **399**, 743–744, 1999.
10. A. Rossi and G.B. Valsecchi, "Self generated debris hazard for satellite constellations", proceedings of the *Second International Workshop on Satellite Constellations and Formation Flying*, Feb. 19–20, 2001, Haifa, Israel, 123–133, 2000.
11. A. Rossi, L. Anselmo, A. Cordelli, P. Farinella P. and C. Pardini, "Modelling the evolution of the space debris population", *Planetary and Space Science*, **46**, 1583-1596, 1998.
12. Su, S.-Y., "The velocity distribution of the collisional fragments and its effect on the future space debris environment", *Adv. Space Res.*, **10**, 389–392, 1990.